A simple model of the large-scale circulation of Mediterranean Water and Labrador Sea Water

Michael A. Spall*

Department of Physical Oceanography, Woods Hole Oceanographic Institution, Woods Hole, MA, 02543, USA

Abstract

A steady, $2\frac{1}{2}$ layer planetary geostrophic model is used to study the circulation and mixing of Mediterranean Water (MW) and Labrador Sea Water (LSW). The model includes para-meterizions of salt fingering, mesoscale variability, and meddies. A close relationship between the vertical density ratio (and expected strength of salt fingering) and the potential vorticity anomaly of the upper salt tongue is identified and used to parameterize salt fingering as a spatially nonhomogeneous diapycnal mass flux. A balance between baroclinic Rossby wave propagation and salt fingering produces an asymmetric tongue of potential vorticity extending into the interior from the eastern boundary, consistent with the observed Mediterranean salt tongue. The resulting internal pressure gradients give rise to a large-scale anticyclonic circulation in the upper layer of the salt tongue with northward flow at mid-latitudes, consistent with geostrophic flow estimates based on hydrographic data. Salt fingering that attains maximum strength at mid-latitudes forces a large-scale circulation in the lower MW/LSW depth range that advects water from the western boundary into the eastern basin near 50°N, where it then flows to the south under the upper MW, and finally returns to the western boundary. This pattern is generally consistent with a variety of estimates for the circulation of LSW, and suggests that the eastward flow of LSW off the western boundary may be, at least in part, forced by salt fingering in the interior. The addition of mixing due to mesoscale eddies modifies the details of the potential vorticity distribution, but does not change the qualitative behavior. Representing meddies as a distributed source of mass to the upper layer results in a further westward extension of the salt tongue signature and enhances the strength of the deep recirculation. © 1999 Elsevier Science Ltd. All rights reserved.

1. Introduction

The warm, salty Mediterranean Water (MW) and the cold, fresh Labrador Sea Water (LSW) are dominant signals at mid-depths in the North Atlantic Ocean. The

* E-mail: mspall@whoi.edu.

MW originates in the Mediterranean Sea and, after mixing with the ambient North Atlantic waters as it flows over the sill in the Strait of Gibraltar, enters the North Atlantic interior centered at a depth near 1000 m. Although the overflow water does not penetrate to great depths, vertical mixing processes in the ocean interior extend this saline signature of the MW to depths greater than 3000 m. The LSW is formed from surface cooling in the Labrador Sea. After being subducted into the ocean interior it resides on density surfaces between approximately 1500 and 3000 m, slightly below the core of the MW. Thus the MW and LSW water influences are found on common density surfaces in the depth range of 1500–3000 m. Although the water masses have distinct source regions and characteristics, mixing in this overlapping region produces water with properties intermediate to the original source waters and makes it difficult to infer the advective pathways based on water mass properties alone.

The basic idea that advective and diffusive components of the flow spread the salty MW from the near coastal region off Portugal into the interior of the North Atlantic has been used by many investigators to study how the salt tongue is maintained. The earliest of these models assumed that salt was a passive tracer and that the velocity field that advects the salinity in the interior was maintained by some means unrelated to the presence of Mediterranean water. Defant (1955) first used an advective/diffusive balance to model the salt tongue. Needler and Heath (1975) assumed a uniform westward flow and observed climatological salinity distribution to estimate the horizontal and vertical diffusivities. Richardson and Mooney (1975) investigated the spread of salinity anomalies from the eastern boundary into the interior under the influences of a wind-driven velocity field and lateral diffusion. Armi and Haidvogel (1982) demonstrated that variable and anisotropic diffusion coefficients could generate tongue-like features in the absence of mean advective fields. More recently, Stephens and Marshall (1998) investigated the steady circulation and salt tongue formation in a $2\frac{1}{2}$ layer planetary geostrophic model with wind forcing, flow through the eastern boundary, and a mass source due to catastrophic breakup of meddies.

Several models of the salt tongue also have assumed that the MW is dynamically active, i.e., that the presence of MW influences the advective and/or diffusive behavior of the flow field. Tziperman (1987) found that a balance between westward Rossby wave propagation and vertical mixing could produce asymmetric tongue-like features when a net mass flux was injected at mid-depths from the eastern boundary. The resulting pressure gradients drive geostrophic flows over depth ranges beyond those at which mass is injected into the interior. Arhan (1987) applied a three-layer planetary geostrophic model to a small region in the interior just west of the Strait of Gibraltar. By representing salt fingering as a downward mass flux from the core of the salt tongue to the layer below, he was able to produce a rotation of the horizonal velocity vector with depth that was consistent with various observations. Spall (1994) used linear theory and nonlinear numerical models to demonstrate that the large-scale meridional flow in the eastern North Atlantic is baroclinically unstable to zonal motions of wavelength $O(100\,\mathrm{km})$, and that the rectified fluxes carried by these unstable waves could represent a significant fraction of the total westward transport of heat and salt.

Because these previous models of the Mediterranean salt tongue, which include both active and passive tracers and a wide range of physics, are able to produce tongue-like features that resemble the distribution of salinity at mid-depths in the North Atlantic, the salinity distribution alone is not sufficient to evaluate which models are most appropriate to the dynamics of the mid-depth circulation. Consideration of the large-scale dynamic height and potential vorticity fields at both the depth of the MW and at deeper depths provides some additional guidelines for the development and evaluation of dynamical models of the mid-depth circulation and salinity budget.

The seminal work of Talley and McCartney (1982) used potential vorticity and salinity to identify three major spreading pathways of LSW away from the Labrador Sea: (1) southward in the Deep Western Boundary Current, (2) northeastward into the Irminger Sea, and (3) eastward along 50°N into the eastern North Atlantic. Observations suggest that much of the eastward branch flows toward the south in the eastern basin, where it appears to become more salty due to mixing with the overlying MW (Wüst, 1935; Talley and McCartney, 1982; Arhan, 1987; Paillet et al., 1998; Cunningham and Haine, 1995). The complexity of these patterns and the multitude of processes that may be important have inhibited the development of simple dynamical models to understand the spreading and mixing of LSW.

It is tempting to attribute the eastward spread of LSW near the subtropical/subpolar gyre boundary and the subsequent southward flow in the eastern North Atlantic to advection by the wind driven flow. However, Armi and Stommel (1983) noted that the beta-spiral balance expected for wind-driven flows in the subtropical gyre was limited to depths above the Mediterranean salt tongue, and that there was a reversal in the vertical shear in the meridional velocity at deeper depths. This pattern of meridional velocities is at odds with what one would expect from a purely wind-driven circulation and suggests that some other process is active in this depth range. Lozier (1997) identifies this eastward and southward flow as part of a basin-scale anticyclonic recirculation and suggests that it may be forced by eddy fluxes along the Gulf Stream and North Atlantic Current. Arhan (1987) concluded that salt fingering from the upper salt tongue into the deeper waters was responsible for the southward flow at depths below the core of the salt tongue. However, Schopp and Arhan (1986) suggested that the northward flow of upper MW is forced by Ekman suction in the subpolar gyre.

The climatological salinity and potential vorticity distributions on $\sigma_1 = 32.0$ (approximately 950 m in the eastern North Atlantic, σ_1 is the potential density referenced to 1000 m) calculated using the Hydrobase data base (Lozier et al., 1995, Curry, 1996) are shown in Fig. 1a. The high salinity waters of the Mediterranean salt tongue are clearly evident, as is the low salinity water originating near the northwestern boundary. Potential vorticity is correlated with these two water masses such that relatively low potential vorticity coincides with the largest salinities and relatively high potential vorticity coincides with the lowest salinities. On a deeper surface, $\sigma_1 = 32.4$ (approximately 1750 m), the high-salinity signature of the Mediterranean water is still evident extending towards the west, however, the potential vorticity of the high-salinity waters at this depth is anomalously high compared to the interior values. It is noted that there is no direct source of high-salinity water on the eastern boundary on this
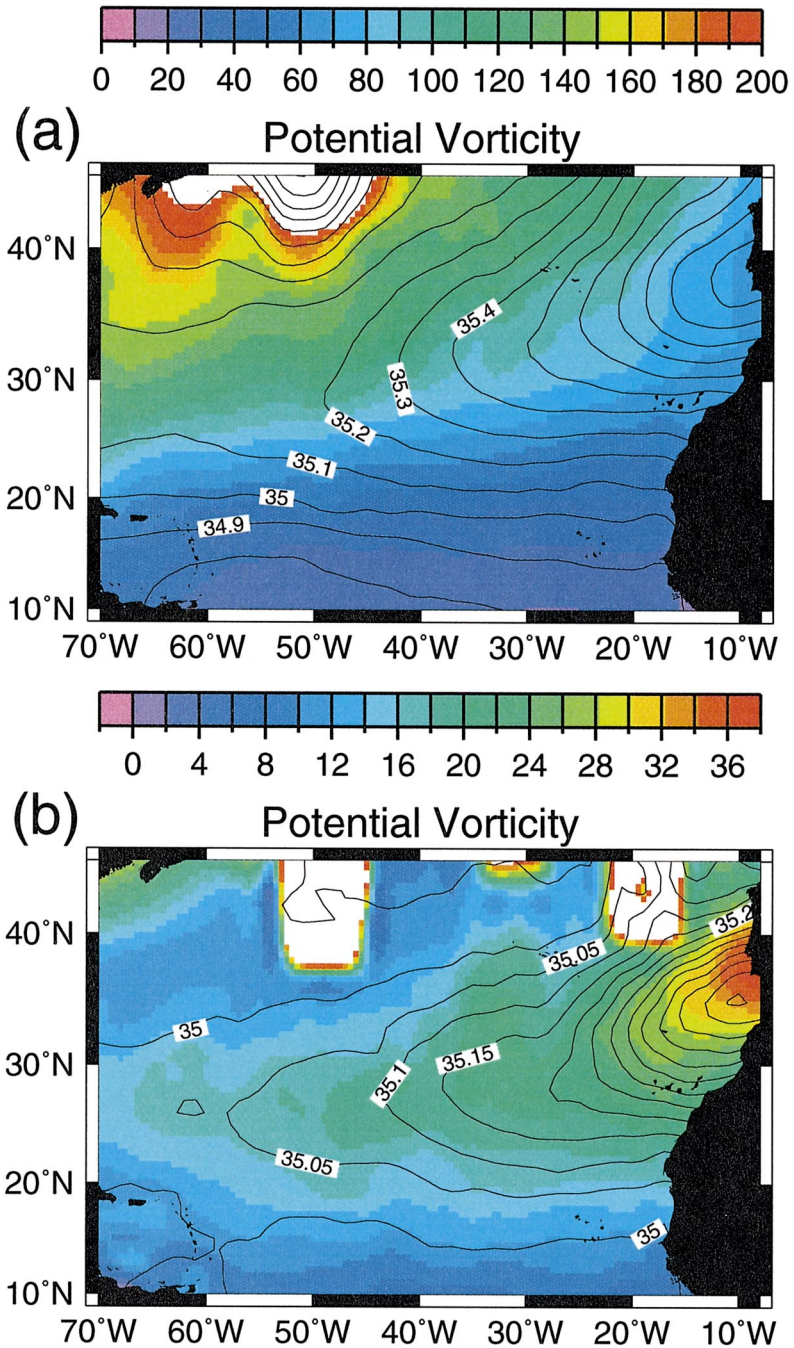
Fig. 1. Salinity contoured with potential vorticity on surface (a) $\sigma_1 = 31.8$ (approximately 750 m in the eastern basin) and (b) $\sigma_1 = 32.4$ (approximately 1700 m in the eastern basin). The high salinity Mediterranean Water corresponds to anomalously low potential vorticity in the upper salt tongue and anomalously high potential vorticity in the lower salt tongue.

isopycnal so that the high salinity found here must have been communicated by vertical mixing with the overlying MW.

This reversal in the zonal gradient in potential vorticity from the upper to the lower waters in the Mediterranean salt tongue is also reflected in the analysis of zonal hydrographic sections east of the Mid-Atlantic Ridge by Saunders (1982). He found that the upper MW was flowing to the north between latitudes 32°N and 48°N, while the lower MW was flowing to the south over the same latitude range. This general flow pattern also is found in the dynamic height calculations of Maillard (1986), reproduced here as Fig. 2. The upper MW is generally flowing to the north, with westward flow near the southern limit of the MW and northeastward flow over the northern extent of the MW. Mazé et al. (1997) find eastward flow of MW in the northern portion of the salt tongue near the eastern boundary. The deeper flow representative of the LSW depths suggests an inflow from the west and north along 50°N, with southward and southwestward flow between latitudes 20°N and 50°N (Fig. 2b). This deep flow pattern is also consistent with the studies of Wüst (1935), Talley and McCartney (1982), Saunders (1982), Cunningham and Haine (1995), Paillet et al. (1998), and Lozier (1997).

The simple model discussed in this paper reproduces many of these large-scale features found in the climatology. However, the model is not intended to realistically simulate all aspects of the mid-depth circulation in the North Atlantic, or to represent all of the physical processes that may be important in determining the large-scale property distributions. The present focus on mid-depth, open-ocean processes provides a complementary approach to previous studies of the North Atlantic circulation and hydrography that have focussed on the main thermocline, western basin, and abyssal oceans. This paper is best viewed as a process-oriented study aimed at gaining
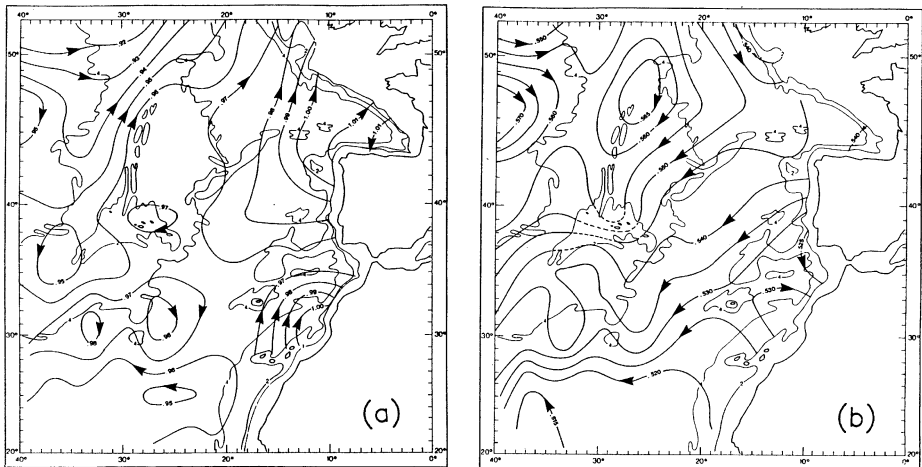
Fig. 2. Dynamic height (in dynamic meters) at 1000 and 1800 m relative to 3000 m (from Maillard 1986). The circulation in the upper salt tongue is generally anticyclonic with northward flow in the interior. A large-scale recirculation is found at deeper depths with inflow near 50°N, southward flow beneath the salt tongue, and westward flow near the southern edge of the salt tongue.

a better understanding of one aspect of what is in the real world a vastly more complex system.

2. The model: equations, boundary conditions, and forcing

The circulation of intermediate and abyssal water masses can be influenced by a wide variety of processes. Several early models of the salt tongue invoked a large-scale circulation consistent with forcing by the surface wind stress. However, estimates of the vertical scale of the wind-driven circulation are typically $O(500\ \mathrm{m})$ and indicate that it is the deepest in the western and northern subtropical gyre (Young and Rhines, 1982). It seems unlikely then that the wind-driven flow could directly influence the circulation in the depth range of the MW and LSW (700–2500 m) in the eastern subtropical gyre (although, as discussed by Young and Rhines (1982) and Stephens and Marshall (1998), the upper ocean wind-driven circulation can distort the potential vorticity contours at the depths of the upper MW). Intermediate and abyssal recirculation gyres can be remotely forced by the wind-driven flow via vertical stresses communicated by mesoscale eddies (i.e., Holland and Rhines, 1980); however, these eddy-driven mean flows are expected to be strongest in the vicinity of separated western boundary currents, and to be very weak in the relatively quiescent eastern subtropical gyre. Mesoscale eddies tend to homogenize the potential vorticity within these deep recirculation gyres (Young and Rhines, 1982); however, the isopycnal surfaces of MW and LSW clearly have large variations in potential vorticity in the vicinity of the salt tongue (Fig. 1). This is in contrast to the smaller scale deep recirculation gyres near the Gulf Stream, in which potential vorticity is homogenized (Lozier, 1997). This suggests that eddy-driven recirculation gyres are not a dominant influence on the spread of MW.

The present model considers the influences of salt fingering, meddies, and mesoscale eddies on the large-scale circulation at mid-depths in the eastern North Atlantic. The focus on these three processes is motivated by their likely importance and the ability to parameterize their effects in terms of the model-dependent variable (potential vorticity).

The model used for this study is essentially the same as the $2\frac{1}{2}$-layer wind and buoyancy driven model introduced by Luyten and Stommel (1986). The stratified ocean is represented as three uniform density layers, the deepest layer assumed to be motionless. The upper active layer represents the upper portion of the Mediterranean Water (MW), approximately $\sigma_1 = 32.0$. The lower active layer represents the density class that contains the deeper portion of the MW and the Labrador Sea Water (LSW), approximately $\sigma_1 = 32.4$.

2.1. Governing equations

The continuity equations for the two moving layers may be written as

$$(hu_1)_x + (hv_1)_y = w_s - w_e + F \tag{1}$$

$$([D - h]u_2)_x + ([D - h]v_2)_y = -w_s - F \tag{2}$$

here u_n and v_n are the zonal and meridional components of the horizontal velocity field in layer n, w_s is a mass flux between layers 1 and 2, and w_e is a mass flux into layer 1 through the upper interface (note that this interface is not intended to represent the ocean surface, but rather the base of the main thermocline at approximately 700 m). The depth of the middle interface is h, and the depth of the lower interface is D.

The present model differs from that of Luyten and Stommel (1986) through the introduction of a parameterization of the eddy induced mass-flux divergence, represented here as F. The eddy fluxes are assumed to act adiabatically to rearrange the position of the interface between layers 1 and 2. For simplicity, it is assumed that the amplitude of the eddy mass flux in both layers 1 and 2 is proportional to the slope of the interface. A similar parameterization for eddy heat flux arising from baroclinic instability has been proposed by Gent and McWilliams (1990). The eddy flux divergence is then proportional to the second derivative of h,

$$F = A_x h_{xx} + A_y h_{yy}, \tag{3}$$

where A_x and A_y are diffusion coefficients in the zonal and meridional directions. This effectively enters the equations as a modification of w_s, even though it is assumed that the eddies act adiabatically. The eddy flux divergence in layer 2 could be related to variations in the thickness of layer 2 $(D - h)$; however, in order to conserve mass this would require motion in the deepest layer, in violation of the assumption of a deep level of no motion.

The velocity field is related to the pressure gradients through the geostrophic relations

$$u_1 = -\frac{g'}{f}(h_y + D_y), \quad v_1 = \frac{g'}{f}(h_x + D_x), \quad u_2 = -\frac{g'}{f}D_y, \quad u_2 = \frac{g'}{f}D_x, \tag{4}$$

where g' is the reduced gravity and $f = \beta y$ is the Coriolis parameter.

Luyten and Stommel (1986) substituted these geostrophic relations into the continuity equations and were able to derive a single first-order partial differential equation that governs the depth of the lower interface D.

$$\left(\frac{fw_e}{\beta D}\right)D_y + \left[-\frac{g'W_{ey}}{fD} - \frac{\beta g'h(D - h)}{f^2 D}\right]D_x = -(w_s + F)\frac{h}{D} \tag{5}$$

The thickness of the upper layer h is related to the depth of the lower interface D and the mass flux through the upper interface as

$$\tfrac{1}{2}(h^2 + D^2) = \tfrac{1}{2}(h_0^2 + D_0^2) + W_e, \tag{6}$$

where h_0 and D_0 are the values of h and D on the eastern boundary. The function W_e is related to the integral of the upper interface mass flux from the eastern boundary $(x = 0)$ to longitude x as

$$W_e = \int_0^x \frac{f^2 w_e}{\beta g'}\,\mathrm{d}x. \tag{7}$$

Luyten and Stommel (1986) assumed that w_e was independent of x and could thus represent this integral explicitly, but the more general form is retained here in order to allow for a longitudinally dependent mass source in the upper layer (meddies).

This system of equations may be solved using the method of characteristics, with the characteristic velocities u_c and v_c given by

$$u_c = -\frac{g'}{f}\frac{W_{ey}}{D} - \frac{\beta g'}{f^2}\frac{h(D-h)}{D}, \quad v_c = \frac{fw_e}{\beta D} \tag{8}$$

The depth of the lower interface changes along the path of the characteristic as a result of the mass flux between the upper and lower layers and the eddy flux divergence:

$$\frac{dD}{ds} = -\frac{h}{D}(w_s + F), \tag{9}$$

where s is the along characteristic distance.

These equations are solved by integrating along characteristics from the boundary of the domain (where h and D are known) into the interior. The depth of the lower interface changes along the path according to the accumulated mass flux into the lower layer, while the thickness of the upper layer is then constrained essentially by the Sverdrup relation through (6). The path of the characteristics is controlled by the characteristic velocities. The sign of the characteristic velocity normal to the boundary determines whether information propagates into the domain (and hence requires the specification of boundary information) or propagates out of the domain, in which case the boundary values are determined from the interior solution. Note that in the absence of a mass source in the upper layer ($w_e = 0$) the characteristic velocities are purely zonal and towards the west. In this limiting case all information originates on the eastern boundary and propagates towards the west at the baroclinic Rossby wave phase speed (zonal advection from the western boundary into the basin interior is still possible in this case).

The parameterization of the eddy mass flux requires that an iterative proceedure be used to solve the equations because the right-hand side of Eq. (9) contains second derivatives of h. An initial guess at the solution is obtained by solving the characteristic equations with $F = 0$ (this gives the same solution as Luyten and Stommel (1986)). These values of h are then used to calculate F from Eq. (3), and the characteristic equations are solved once again with the estimated value of F used on the right-hand side of Eq. (9). This procedure is repeated until the maximum change in h between successive iterations is less than 10^{-2} m.

2.2. Boundary conditions

The depths of the upper and lower interfaces need to be specified on all incoming characteristics. For all problems considered here the mass source in the upper layer (w_e) is always sufficiently small that all characteristics originate from the eastern

boundary. The dynamics that control the initial spreading of MW from the near outflow region and along the eastern boundary into the interior are very complex involving turbulent entrainment, mesoscale eddies, meddies, fronts, and topographic influences (Käse and Zenk (1996) and the references therein). The large-scale geostrophic dynamics of this model are not appropriate for the near coastal region, or the immediate vicinity of the overflow through the Strait of Gibraltar, and so the eastern boundary of the model is taken to be a meridional section in the interior of the ocean, away from the near coastal region, where the large-scale dynamics are appropriate. Flow is allowed through the eastern boundary of the model because it is not intended to represent a solid wall. A similar eastern boundary condition was applied by Arhan (1987).

Estimates of geostrophic transports between the near coastal region and the deep ocean based on synoptic sections are often dominated by mesoscale variability and the choice of reference level (Arhan et al., 1994; Käse and Zenk, 1996). While mesoscale eddies are probably an important exchange mechanism between the near coastal region and the deep ocean, the boundary condition for the large-scale planetary geostrophic model used here needs only reflect the net influence of these small-scale processes on the large-scale potential vorticity structure along the eastern boundary. This large-scale signature is best revealed by considering the average over many independent observations, as in the climatological hydrography (Fig. 1). The presence of salty, low potential vorticity water along the eastern boundary is represented in the model by specifying that the thickness of layer 1 increase at the latitudes where the MW is introduced to the ocean interior. The general solution characteristics are not overly sensitive to the specific meridional distribution, so long as it has a local maximum in layer thickness at mid-latitudes. Two particular forms of the eastern boundary condition will be used here.

The boundary condition for the central calculation (boundary condition A) specifies that the thickness of layer 1 along the eastern boundary has a local maximum at mid-latitudes as

$$h_0(y) + \bar{h} + h' \cos\left(\pi \frac{y - y_m}{L_y}\right), \quad y_m - \frac{L_y}{2} < y < y_m + \frac{L_y}{2}, \tag{10}$$

$$h_0(y) = \bar{h}, \quad y < y_m - \frac{L_y}{2}, \quad y > y_m + \frac{L_y}{2}, \tag{11}$$

where $\bar{h}$ is the thickness of layer 1 away from any MW influence, h' is the maximum thickness anomaly associated with MW, y_m is the latitude of maximum MW influence on the eastern boundary, and L_y is the meridional scale of the Mediterranean salt tongue on the eastern boundary.

The climatological salinity and potential vorticity distributions in Fig. 1 suggest a presence of MW in the upper layer along the eastern boundary to the north of the maximum MW influence. A second boundary condition (boundary condition B) also is used in which the thickness of layer 1 along the eastern boundary does not decrease

north of the latitude of maximum MW influence.

$$h_0(y) = \bar{h} + h' \cos\left(\pi \frac{y - y_m}{L_y}\right), \quad y_m - \frac{L_y}{2} < y < y_m, \tag{12}$$

$$h_0(y) = \bar{h}, \quad y < y_m - \frac{L_y}{2}, \tag{13}$$

$$h_0(y) = \bar{h} + h', \quad y > y_m. \tag{14}$$

This anomalously low potential vorticity along the eastern boundary represents the northward flow of MW by eastern boundary currents.

The boundary condition for the second layer is no flow through the eastern boundary. This layer is sufficiently dense that the end product of the mixing between the water that flows through the Strait of Gibraltar and the ambient North Atlantic water is lighter than this layer, and no mass is introduced from the coastal region along the eastern boundary. At the northern and southern limits of the model domain $w_e = 0$, the characteristics are purely zonal, and thus there is no need to independently specify h or D along the northern and southern boundaries as they are calculated as part of the solution. The intent here is not to construct the most realistic circulation model possible (in which case one would want to consider influences from the adjacent gyres and western basin processes), but rather to consider the circulation patterns and potential vorticity distributions that arise from a single source on the eastern boundary. Thus, the boundary condition on D is $D_0(y) = \bar{D}$.

2.3. Forcing

The only imposed forcing mechanisms in the model are represented by the interfacial mass fluxes w_e and w_s. While diapycnal mixing in the ocean interior is generally believed to be small ($O(10^{-5}\,\text{m}^2\,\text{s}^{-1})$, Ledwell et al., 1993), salt fingering can result in diapycnal diffusion coefficients as large as $10^{-3}\,\text{m}^2\,\text{s}^{-1}$ (Schmitt, 1981). Climatological hydrography, as well as synoptic surveys (Washburn and Käse, 1987; Arhan, 1987; Tsuchya et al., 1992; Daniault et al., 1994), and microstructure data (Magnell, 1976; Williams, 1975) suggest that the Mediterranean salt tongue is a region of active salt fingering. Because of this large difference in mixing coefficients, and for simplicity, the only diapycnal mass flux included in the model is a parameterization of salt fingering. Tziperman (1987) considered spatially varying upwelling in the interior. While meddies are generally thought to be important in the salinity budget in this region (Richardson et al., 1991; Bower et al., 1997; Käse and Zenk, 1996), their influence on the large scale circulation and property distribution has not yet been represented in dynamical models of the salt tongue.

2.3.1. Salt fingering
Salt fingering diffuses salinity and heat downward at different rates, resulting a negative vertical diffusivity for density (Schmitt, 1981). If one invokes the traditional

one-dimensional vertical heat balance across isopycnal surfaces, this requires a downward vertical velocity to balance the upward diffusion of density by salt fingering. The diapycnal velocity scales as $w_s = \kappa/H$, where $\kappa < 0$ is the vertical diffusion coefficient and H is a vertical scale height. Thus, the effect of salt fingering is represented in the layered model by transferring mass from the upper layer of the salt tongue to the lower layer. Arhan (1987) also imposed a negative vertical velocity to represent salt fingering in a local model of the salt tongue; however, he assumed that salt fingering was uniformly active over the entire region of the model domain. It is well known that the strength of vertical diffusion resulting from salt fingering activity is a strong function of the vertical density ratio $R_\rho = \alpha T_z/\beta S_z$, where α and β are thermal and saline expansion coefficients (Schmitt, 1981). Arhan recognized this limitation, but lacked a means to determine the spatial variability in the strength of salt fingering because the model did not carry salinity as a variable and thus had no way to distinguish Mediterranean water from ambient North Atlantic water.

The simple model used here also does not carry salinity, but it does carry potential vorticity. The apparent correlation between salinity and potential vorticity in Fig. 1 suggests that one might be able to parameterize salt fingering in terms of the potential vorticity field. The Hydrobase climatology averaged into $2° \times 2°$ bins shows that the potential vorticity anomaly in the upper salt tongue ($\sigma_1 = 32.0$) is nearly linearly related to salinity such that very salty water has an anomalously low potential vorticity (Fig. 3a). The potential vorticity anomaly is used, rather than potential vorticity, in order to subtract out the effect of variations in planetary vorticity.

Because the large-scale potential vorticity is inversely related to the thickness of an isopycnal layer, a similar linear relationship exists between salinity and the thickness anomaly (Fig. 3b). The maximum thickness anomaly in the upper salt tongue is approximately 150 m and corresponds to the core of the salt tongue where the salinity is the largest. This systematic variation in layer thickness with salinity suggests that the MW is not dynamically passive but that large-scale pressure gradients and geostrophic currents are associated with its potential vorticity signature, independent of the upper ocean circulation and wind-stress curl at the surface.

The vertical density ratio also has been calculated from the hydrographic data between density surfaces $\sigma_1 = 32.35$ (approximately 1500 m in the eastern basin) and $\sigma_1 = 32.4$ (approximately 1750 m). This density range was chosen to represent the lower portion of the salt tongue, where salt fingering is expected to be most active. This density ratio is plotted against the salinity in the upper core ($\sigma_1 = 32.0$) in Fig. 3c. Salt fingering is expected to be most active between $1 < R_p < 2$, with the strongest salt fingering as $R_p \to 1$. There is a clear trend towards lower density ratio with increasing salinity.

Finally, the density ratio in the lower salt tongue decreases with increasing thickness anomaly in the upper salt tongue (Fig. 3d). The thickness anomaly of the upper layer is used, rather than in the core, because the zonal potential vorticity gradient changes sign (zero thickness anomaly) at mid-depths. Although there is no direct dynamical connection between the density ratio at depth and the stratification in the upper layer, the thickness anomaly (or salinity) of the upper layer is an effective index
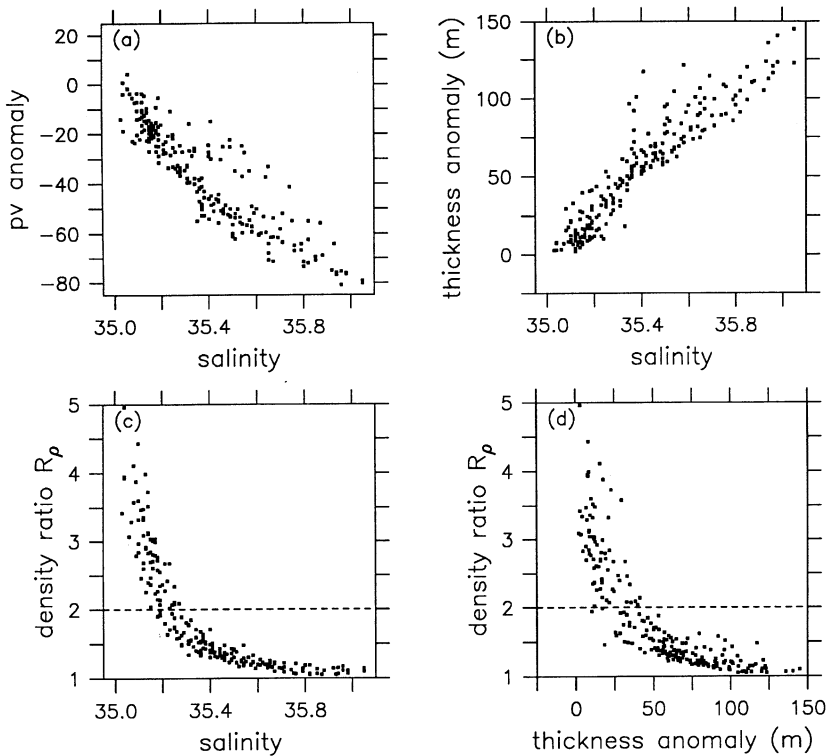
Fig. 3. Data points taken from the Hydrobase climatology (Lozier et al., 1995), averaged into 2° bins between 26°N, 50°N, and bounded by the 35.0 ppt salinity contour or 75°W to the west. (a) Potential vorticity anomaly versus salinity on surface 32.0, (b) thickness anomaly between isopycnal surfaces $\sigma_1 = 31.8$ and $\sigma_1 = 32.0$ versus salinity, (c) density ratio $R_\rho = \alpha T_z / \beta S_z$ in the lower salt tongue ($\sigma_1 = 32.35$) versus salinity, and (d) density ratio versus thickness anomaly. The potential vorticity and thickness anomalies are defined as the difference between the local value and the value at the same latitude on the 35.0 ppt salinity contour (or at 75°W in the event that the 35.0 contour is not encountered). There is a nearly linear relationship between salinity and the potential vorticity and thickness anomalies. The density ratio is greater than 2 (weak salt fingering) for low salinities and approaches 1 (strong salt fingering) for high salinities. The density ratio is related to the thickness anomaly such that strong salt fingering is expected in regions where the upper layer thickness is large (potential vorticity is low). This relationship forms the basis for the parameterization of salt fingering in the model (15).

for locating the position of the salt tongue, and is thus also a good indicator of the expected strength of salt fingering at the base of the salt tongue.

While the specific functional relationship between diffusivity and density ratio is not well known, the general trend is that the amplitude of the vertical diffusivity increases with decreasing density ratio (Schmitt, 1981; Zhang et al., 1997). The vertical diffusivity is linearly related to the diapycnal mass flux w_s in the model (assuming uniform scale height). The results in Fig. 3 suggest a simple parameterization of salt fingering, where the diapycnal mass flux w_s is linearly proportional to the layer thickness

anomaly as

$$w_s = w_{s0} \frac{h(x, y) - \bar{h}}{h'}. \tag{15}$$

The diapycnal velocity attains its maximum of w_{s0} for the strongest signature of MW ($h = \bar{h} + h'$), while it decreases to zero at the edges of the Mediterranean salt tongue where $h = \bar{h}$. The simple form (15) captures the most basic elements of the relationship between the water mass properties and the expected diapycnal mass flux. More sophisticated parameterizations of course could be incorporated; however, only a qualitative understanding of the relationship between salt fingering and the large-scale circulation is sought here. A quadratic relationship also has been tested and gives results that are qualitatively similar to those reported here. A guideline for the maximum amplitude of the diapycnal mass flux that can be expected due to salt fingering is provided by the recent parameterization proposed by Zhang et al. (1997). While their exact formula is more sophisticated than is warranted for the present idealized model, they estimate that the diapycnal diffusivity for density is approximately $-3 \times 10^{-4} \, \text{m}^2 \, \text{s}^{-1}$ for a density ratio of 1.1. This can be converted to a diapycnal mass flux by dividing by the layer thickness, $O(10^3 \, \text{m})$, giving $w_{s0} = O(-3 \times 10^{-7} \, \text{m} \, \text{s}^{-1})$, similar to the values used by Arhan (1987).

2.3.2. Meddies

Meddies (lenses of Mediterranean salt water) are believed to be formed near Cape St. Vincent (Bower et al., 1997), and are most often found in the region extending to the southwest between 25°N and 45°N, and as far west as 30°W (Richardson et al., 1991). Meddies propagate as coherent vortices and transport mass, salinity, and potential vorticity from the boundary region into the basin interior. As the meddies decay, they deposit their salinity and mass into the large-scale flow. The mass flux carried into the interior of the basin by meddies is estimated to be $O(0.5–1 \, \text{Sv})$ (Bower et al., 1997), carrying approximately 25% of the total MW salinity anomaly into the interior (Richardson et al., 1989). The mass flux due to decaying meddies is parameterized as a distributed mass source in layer 1 through the specification of w_e.

The dynamics that control the propagation pathways and decay rates of meddies are quite complicated (involving beta-plane vortex dynamics, interactions with the upper ocean, the Azores Current, and topography, small scale turbulence and mixing (Käse and Zenk, 1996), and no attempt is made to resolve explicitly these processes here. The survey of historical hydrographic data by Richardson et al. (1991) suggests a simple distribution of a mass source w_e to represent the large-scale distribution of decaying meddies as

$$w_e(y) = w_{e0} \exp\left\{ -\frac{(y - y_\text{m})^2}{L_\text{m}^2} \right\}, \quad x > x_\text{m}, \tag{16}$$

$$w_e(y) = 0, \quad x < x_\text{m}.$$

where w_{e0} is the maximum strength of the mass source, L_m is the meridional length scale over which the meddies are found and x_m is the westernmost extend of the

meddies. The mass source from meddies decreases exponentially to the north and south from its maximum along the latitude $y = y_m$. The maximum strength of the mass source may be related to the number of meddies formed per year and their characteristics as

$$w_{e0} = -\frac{\sqrt{\pi} N h_m r_m^2}{3.156 \times 10^7 x_m L_m} \tag{17}$$

where N is the number of meddies formed per year, h_m and r_m are the thickness and radius of the meddies, and 3.156×10^7 is the number of seconds in a year. While this parameterization is very crude, the intent here is only to gain a qualitative under-standing of how decaying meddies influence the large-scale circulation and distribu-tion of potential vorticity.

3. Model results

3.1. Salt fingering

The central calculation considers only the influences of salt fingering and the advective field generated by the internal pressure gradients associated with the spread of the low potential vorticity signal into the interior. The upper layer has an ambient layer thickness of $\bar{h} = 600$ m, and the depth of the lower interface along the eastern boundary $\bar{D} = 1800$ m. Recall that these values are taken relative to the top of the Mediterranean salt tongue, which is at a depth of approximately 700 m in the eastern North Atlantic Ocean. The maximum thickness anomaly in the upper layer is $h' = 150$ m. The potential vorticity anomaly on the eastern boundary is centered at $y_m = 35°$N and has a meridional extent of $L_y = 4 \times 10^6$ m. The maximum diapycnal velocity associated with salt fingering is $w_{s0} = -4 \times 10^{-7}$ m s^{-1}. The variation in the Coriolis parameter with latitude $\beta = 2 \times 10^{-11}$ m^{-1} s^{-1}, and the reduced gravity $g' = 0.004$ m s^{-2}. The upper active layer represents the upper core of the Mediterranean salt tongue ($\sigma_1 = 32.0$, depth range 700–1300 m), and the lower active layer represents the deep MW and LSW ($\sigma_1 = 32.4$, depth range 1300–2500 m).

3.1.1. Circulation of MW

The signature of the low potential vorticity water extends into the basin interior with increasing westward penetration towards the south (Fig. 4a). The latitude of maximum potential vorticity anomaly (analogous to salinity) shifts to the south as the tongue extends offshore. The total southward shift of the core of the tongue is approximately 12° of latitude, similar to that found in the climatology in Fig. 1. The penetration scale of the anomalous water is determined from the balance between the westward propagation of information at the baroclinic Rossby wave speed and the erosion of this signal by salt fingering. This balance may be used to obtain an estimate of the zonal length scale L_x over which the eastern boundary potential vorticity
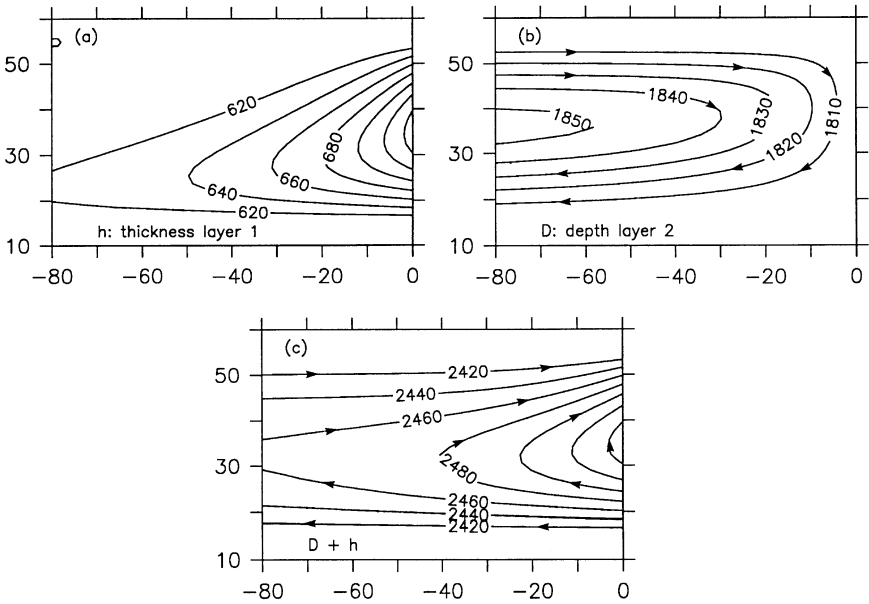
Fig. 4. Calculation with salt fingering ($w_{s0} = -4 \times 10^{-7}\,\mathrm{m\,s^{-1}}$) and a finite northward extent of MW on the eastern boundary (boundary condition A, Eqs. (10) and (11)). (a) Thickness of layer 1, (b) depth of the deep interface D, (c) streamlines for layer 1 circulation $h + D$ (arrows in (b) and (c) indicate flow direction).

anomaly will extend into the interior [making use of Eqs. (6), (8), and (9)] as

$$L_x = \frac{\beta g' h'(\bar{D} - \bar{h})\bar{h}}{\bar{D} w_{s0} f^2}. \tag{18}$$

This length scale may be interpreted as the product of the Rossby wave phase speed and the vertical diffusive time scale. The anomalous water mass properties extend further into the basin at lower latitudes because Rossby wave phase speed scales with f^{-2}. This balance is similar to the damped Rossby wave length scale found in the idealized model of the Mediterranean salt tongue by Tziperman (1987), where only the lowest baroclinic vertical mode is represented here.

  The depth of the lower interface deepens to the west (Fig. 4b), as required by the downward mass flux due to salt fingering (9). The total increase in the depth of the lower interface is only $O(50\,\mathrm{m})$ over the entire width of the basin; however, we will see that this slight variation in pressure will give rise to significant transports in both the upper and lower portions of the Mediterranean salt tongue.

  The flow direction in the upper layer, given by the geostrophic relations (4), is in the direction of isolines of $D + h$ (Fig. 4c). There is a westward flow in the southern salt tongue and towards the east in the northern salt tongue. The interior of the salt tongue supports a very weak northward flow of $O(0.1\,\mathrm{cm\,s^{-1}})$ with anticyclonic rotation, consistent with the geostrophic estimates of Saunders (1982), and in general

agreement with the dynamic height calculations of Maillard (Fig. 2). The inverse model of Paillet and Mercier (1997) shows no clear northward flow at 1000 m. The flow into the eastern boundary in the northern portion of the salt tongue is consistent with the eastward transport of MW of $O(0.5 \text{ Sv})$ found by Mazé et al. (1997) between latitudes 37°N and 43°N at 12°30′W. However, it is emphasized here that the strength, or even direction, of the mean circulation at the depths of the upper MW are not well known.

The circulation predicted at the depths of the salt tongue by the inverse model of Hogg (1987) is generally to the west between latitudes 23°30′N and 41°30′N and west of 23°30′W. While this is consistent with the circulation implied in Figs. 2 and 4, the inverse model was not applied further to the north and east, where the northward flow of MW is expected to be strongest.

The meridional transport is forced by the erosion of the low potential vorticity anomaly as it penetrates into the interior. The zonal transports are supported by the small variations in the depth of the lower interface that, through the thermal wind relation, are communicated to the upper layer. The zonal transport to the western boundary in layer 1 (Γ_1) is estimated from the basic model parameters to be

$$\Gamma_1 = \frac{g'(h' + \bar{h})\bar{h}h'}{2D_0 f} \approx \frac{g'h'\bar{h}^2}{2D_0 f}. \tag{19}$$

It is clear that there will be a net loss to the western boundary because more transport is achieved at lower latitudes than at higher latitudes for the same pressure gradient. Taking a representative low latitude value for the Coriolis parameter at $f = 0.4 \times 10^{-4} \text{ s}^{-1}$, this gives a westward transport of approximatly 2 Sv ($1 \text{ Sv} = 10^6 \text{ m}^3 \text{ s}^{-1}$). The eastward transport at higher latitudes is estimated with $f = 0.8 \times 10^{-4} \text{ s}^{-1}$ to be 1 Sv, resulting in a net flux into the western boundary region of approximately 1 Sv. The ultimate fate of this water is not determined in this simple model, but it is expected that this water would be transported meridionally in the western boundary current system. The main point here is not to be quantitative in estimating these transports, but to point out that an asymmetry exists that would result in a net transport to the west. A similar asymmetric circulation pattern is estimated from hydrographic data by Saunders (1982).

There is also a net flux of mass from layer 1 into layer 2 due to salt fingering. This total conversion is calculated by integrating the mass flux due to salt fingering over the spatial area of the salt tongue. The conversion found in the central calculation is 2.6 Sv. It is important to note that the total mass conversion (and the strength of the deep recirculation) are independent of the strength of the diapycnal mixing, or its detailed parameterization, provided that the mixing erodes the potential vorticity anomaly before it reaches the western boundary. This is because the area over which the integral is taken is inversely proportional to the strength of the diapycnal mixing (stronger mixing results in a smaller region of salt fingering). It also does not depend on how the low potential vorticity water in layer 1 was transported into the interior.

3.1.2. Circulation of LSW

The pattern of circulation in the lower layer is along lines of constant D (Fig. 4b). The sense of the circulation is anticyclonic with eastward flow in the northern half of the basin and westward flow in the southern half. The meridional flow is to the south in the interior of the basin at mid-latitudes. This pattern is in general agreement with the southward meridional flow of Saunders (1982), and the zonal penetration near 50°N and southward recirculation of LSW described by Talley and McCartney (1982), Paillet et al. (1998), and Cunningham and Haine (1995). A similar anticyclonic basin-scale recirculation, with flow returning to the western boundary region at low latitudes, is indicated in the geostrophic flow calculations of Lozier (1997). In contrast, a model with upwelling in the interior will produce northward flow everywhere in the interior, as found by Tziperman (1987).

The deep circulation in the model is forced by the diapycnal mass flux associated with salt fingering. The pattern of a large-scale anticyclonic recirculation arises because salt fingering is active only in the mid-latitudes where the MW is present in the upper layer. The linear vorticity balance requires that there be southward flow under the region of salt fingering, and purely zonal flow (as required for mass conservation) at high and low latitudes at which there is no salt fingering. This spatially variable parameterization of salt fingering extends the local circulation balance described by Arhan (1987) to the basin-scale, where a new, large-scale circulation emerges that connects the western boundary to the eastern basin in both the north and south.

This deep recirculation is also necessary in order to remove the downward mass flux resulting from salt fingering. For a no-flow condition through the eastern, southern, and northern boundaries, there can be no net pressure gradient across the latitude range of the salt tongue. By developing a basin-scale recirculation, the system is able to export the mass introduced into the lower layer, but only by importing water from the western boundary at higher latitudes. There is a net transport to the west because f increases with latitude. The ratio R of the strength of the recirculation to the net conversion is estimated (for $y_m > L_y/2$) to be

$$R \approx y_m/L_y + \tfrac{1}{2}. \tag{20}$$

The relative strength of the anticyclonic recirculation increases as the meridional scale of the region of diapycnal mass flux decreases because the change in f across the forcing region becomes small. This is similar to the problem discussed by Pedlosky (1996) for localized buoyancy forcing on a sphere. For the parameters appropriate to the Mediterranean salt tongue, $L_y \approx y_m$ and the strength of the recirculation is similar to the total water mass converted from the upper layer into the lower layer. For the parameter values used in Fig. 4, a total of 2.7 Sv of water is advected from the western boundary into the interior between latitudes 41°N and 60°N. This is similar to the 3.1 ± 1 Sv of LSW estimated by Paillet et al. (1998) to be advected eastward along 50°N and southward east of the Mid-Atlantic Ridge. The westward flow in layer 2 between 15°N and 35°N is the sum of the LSW advected eastwards in the Northern half of the domain (2.7 Sv) and the mass flux mixed downward due to salt fingering (2.6 Sv), giving a total westward transport of 5.3 Sv.

The eastward flow out of the western boundary is required by the dynamics in the interior of the basin, it is not dictated by processes near the western boundary. This invites the interpretation that the eastward spreading of LSW and its southward recirculation in the eastern North Atlantic is "pulled" by the salt fingering in the interior rather than "pushed" by the eastward advection at the subtropical/subpolar gyre boundary, particularily since there are no wind-driven gyres in the present model. It is difficult, however, to separate the interior/western boundary influences so easily because it has been assumed from the outset that the presence of low potential vorticity water in the eastern basin is coincident with active salt fingering. In order to maintain this state in the real ocean, a continual supply of fresh water and a means to get rid of the downward flux of salt are required. If there were no such supply of fresh water available along the north western boundary, the deep eastern North Atlantic would presumably become sufficiently salty that the salt fingering would shut down, and the forcing in the model would no longer be appropriate.

The erosion of the MW signal as it penetrates into the basin interior gives rise to a negative zonal gradient in the potential vorticity in the upper layer and a positive gradient in the lower layer. This potential vorticity structure is qualitatively consistent with the reversal found in the climatological hydrography (Fig. 1), and is necessary to support the reversal in the vertical shear of the meridional velocity reported by Saunders (1982), Armi and Stommel (1983), Maillard (1986), and Arhan (1987). This basic potential vorticity structure is reproduced here even without an explicit source of LSW, once again suggesting that the presence of low potential vorticity water in the western deep layer is required by the interior dynamics, rather than being forced by western boundary layer processes.

3.1.3. Sensitivity to the eastern boundary condition

The layer thicknesses resulting from imposing MW in the upper layer all the way to the north along the eastern boundary [boundary condition B, Eqs. (12)–(14)] are shown in Fig. 5. The solution to the south of latitude y_m is identical to the previous calculation (recall that for these cases the characteristics are purely zonal). There is still an asymmetric meridional distribution of the upper layer thickness except that now the thickness contours are nearly parallel to the eastern boundary as they extend to the north. The direction of deep circulation (indicated by the depth of the lower interface in Fig. 5b) is to the south at latitudes where there is a MW influence and to the west at low latitudes. The southward-flowing current narrows to the north because the Rossby wave propagation speed decreases with increasing latitude (see also Tziperman, 1987). The total southward transport is uniform with latitude north of y_m because the layer thickness eroded by salt fingering is uniform with latitude (this change in layer thickness balances the meridional flow). All of the upper layer MW flows to the north at high latitudes (Fig. 5c) instead of returning to the eastern boundary as it did in the central calculation. This solution reproduces some aspects of the dynamic height calculations of Maillard (Fig. 2) better than the central calculation, such as the southward flow in the lower layer at 50°N.

The boundary conditions used here are not intended to provide the most realistic representation of the observations, but rather to demonstrate the range of possible
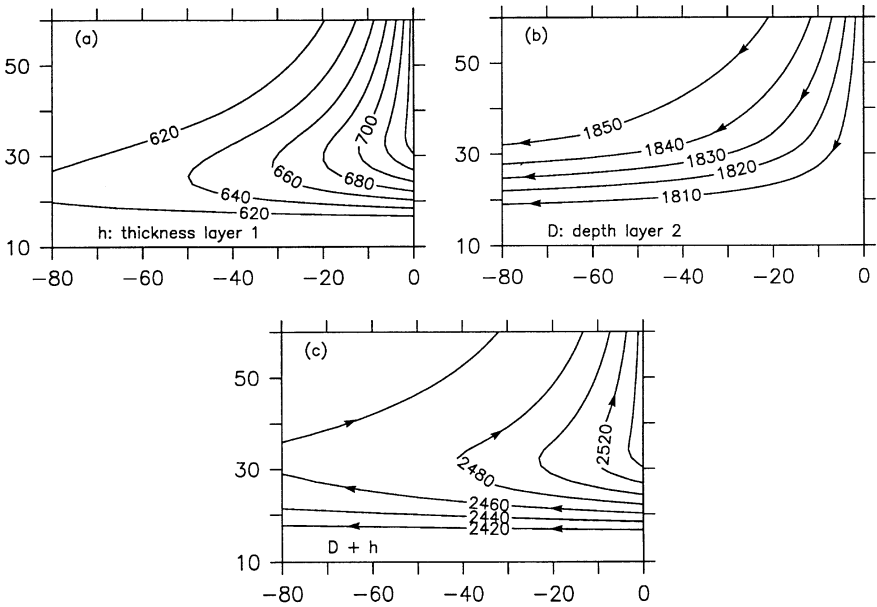
Fig. 5. Calculation with salt fingering ($w_{s0} = -4 \times 10^{-7}\,\text{m s}^{-1}$) and MW imposed along the eastern boundary north of y_m (boundary condition B, Eqs. (12)–(14)) (a) Thickness of layer 1, (b) depth of the deep interface D, (c) streamlines for layer 1 circulation $h + D$ (arrows in (b) and (c) indicate flow direction).

solutions and the sensitivity of the circulation to latitudinal variations in salt fingering. If there is a local maximum in the zonally integrated diapycnal mass flux due to salt fingering within the latitude range of the salt tongue (boundary condition A), then LSW will be advected from the western boundary into the eastern basin. If there is no decrease in the total strength of salt fingering with increasing latitude (boundary condition B), then the LSW will be advected into the eastern basin from the north. Eastern boundary conditions intermediate to the two discussed here produce a deep circulation in which some of the deep transport originates from the western boundary and some originates in the north, similar to the circulation in Fig. 2.

3.2. Mesoscale eddies

The influence of mesoscale eddies is now added to the central calculation. The diffusion coefficients are taken to be larger in the zonal direction ($A_x = 2000\,\text{m}^2\,\text{s}^{-1}$) than in the meridional direction ($A_y = 1000\,\text{m}^2\,\text{s}^{-1}$). While there is some uncertainty in setting specific values, these represent an upper bound on various estimates published in the literature (Freedland (1975) $700\,\text{m}^2\,\text{s}^{-1}$, Armi and Stommel (1983) $500\,\text{m}^2\,\text{s}^{-1}$, Hogg (1987) $O(500\,\text{m}^2\,\text{s}^{-1})$, Spall et al. (1993) $A_x = 2100\,\text{m}^2\,\text{s}^{-1}$, $A_y = 840\,\text{m}^2\,\text{s}^{-1}$). Although there is some evidence for spatial inhomogeneity in the diffusion coefficients (Spall et al., 1993), and this can influence the shape of the salt tongue (Armi and Haidvogel, 1982), constant coefficients are chosen here for simplicity.
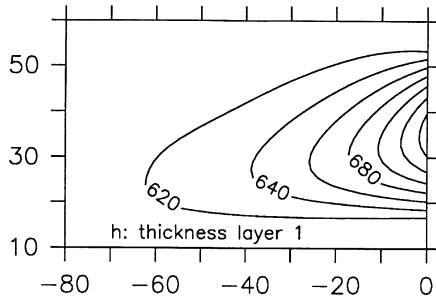
Fig. 6. Thickness of layer 1 for a case with salt fingering and a horizontal diffusive parameterization of mesoscale eddies ($A_x = 2000 \, \mathrm{m^2 \, s^{-1}}$, $A_y = 1000 \, \mathrm{m^2 \, s^{-1}}$). The mesoscale eddies enhance the meridional and limit the westward spread of MW.

The influence of the eddies is primarily to spread the MW in the meridional direction and to reduce the north–south asymmetry, despite the larger diffusion coefficient in the zonal direction (Fig. 6). In fact, there is less zonal penetration of the low potential vorticity water in the presence of horizontal diffusion because of the meridional spreading (there is no longer a simple balance between Rossby wave propagation and diapycnal mixing). The eddy flux divergence is small compared to the diapycnal mass flux due to salt fingering over most of the salt tongue, so the influence of mesoscale eddies is relatively small compared to that of salt fingering. The remaining properties of the solution (depth of the deep interface, potential vorticity distributions, circulation patterns and amplitudes) are quite similar to the central case and are not shown.

This parameterization probably underestimates the importance of mesoscale eddies in the salt tongue balance because they are very important for determining the distribution of salinity and potential vorticity along the eastern boundary region (Käse and Zenk, 1996). This eastern boundary condition is imposed on the model without distinguishing what physical processes are important in determining how the MW gets from the near coastal region into the basin interior, thus it is difficult to fully remove their influence from the calculation.

3.3. Meddies

The influence of meddies is now added as a distributed mass source in the upper layer. The lateral diffusion coefficients A_x and A_y are both zero in this calculation. There is a great deal of uncertainty in setting the parameters to define how many meddies are formed and where they decay; however, the main intent here is to investigate their qualitative influence on the large-scale potential vorticity distribution and circulation patterns in the Mediterranean salt tongue. It is assumed that 20 meddies are formed per year, each of thickness 1000 m and radius of 20 km (Bower et al., 1997). This results in a total mass flux into layer 1 by meddies of 0.8 Sv. The zonal decay scale $x_m = 3 \times 10^6$ m and the meridional decay scale $L_m = 1 \times 10^6$ m, resulting in $w_{e0} = -1.5 \times 10^{-7} \, \mathrm{m \, s^{-1}}$.
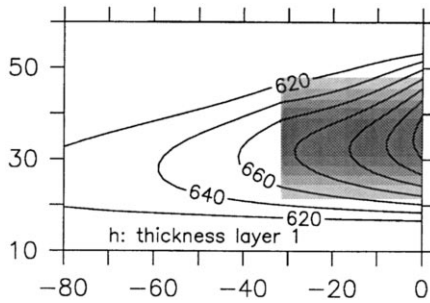
Fig. 7. Thickness of layer 1 for a case with salt fingering and a distributed mass source due to meddies. The primary influence of meddies is to enhance the westward extent of the salt tongue and strengthen the deep recirculation gyre (not shown). Shading indicates the region of meddy decay, the maximum value of w_e ($-1.5 \times 10^{-7}\,\mathrm{m\,s^{-1}}$) occurs at $y = 35$.

The primary influence of the meddies is to extend the signature of the salt tongue approximately 750 km to the west (Fig. 7). The decaying meddies increase the thickness of the upper layer (relative to the case with no meddies) in the region east of x_m. The additional mass flux supplied by the meddies gets mixed downward by salt fingering. The strength of the deep recirculation is now 3.5 Sv, the increase of 0.8 Sv from the case with no meddies is essentially equivalent to the mass flux of the meddies, as expected from Eq. (20). These changes in the strength and scale of the circulation are consistent with estimates that meddies transport approximately 25% of the MW salinity anomaly into the basin interior (Richardson et al., 1989). The remaining properties of the solution (depth of the deep interface, deep circulation pattern, potential vorticity distributions) are quite similar to the previous case and are not shown.

Calculations with boundary condition B produce a deep circulation in which most of the flow in the deep layer originates from the north, while the amount required to balance the downward flux resulting from meddies enters through the western boundary just to the north of the meddy decay region.

As with the meoscale eddies, it is difficult to fully eliminate the influences of meddies from the calculation because they are, at least indirectly, represented in the eastern boundary condition imposed on the model.

4. Summary

A simple, steady theory for the large-scale circulation of Mediterranean Water and Labrador Sea Water at mid-depths in the North Atlantic is presented. The model is very idealized, but includes parameterizations of salt fingering, mesoscale eddies, and meddies, as well as advection by the geostrophic flow. A relationship between the vertical density ratio and the potential vorticity anomaly is used to parameterize salt fingering as a spatially nonhomogeneous diapycnal mass flux. This is a key difference between this model and previous models of the salt tongue.

The circulation in the model is determined primarily by large-scale spatial variations in the strength of salt fingering and the eastern boundary condition, with some quantitative differences resulting from the addition of mixing due to mesoscale eddies or a distributed mass source representative of meddies. A balance between westward propagation by baroclinic Rossby waves and vertical diffusion by salt fingering produces an asymmetric tongue of low potential vorticity water consistent with the potential vorticity distribution in the Mediterranean salt tongue. The resulting internal pressure gradients produce a circulation that generally agrees with some estimates based on climatological hydrography. Two important aspects of the flow field are a northward flow in the upper portion of the Mediterranean salt tongue, and a deep anticyclonic recirculation of Labrador Sea Water. While it is difficult to demonstrate that wind and buoyancy forcing from the upper ocean or eddy-driven recirculation gyres are not important, many aspects of the large-scale circulation are reproduced in this model in the absence of any upper ocean forcing. This suggests that the eastward flow of LSW near 50°N, its southward flow east of the mid-Atlantic Ridge and westward return flow may be forced by salt fingering under the upper MW in the salt tongue.

This large-scale recirculation of LSW provides a direct pathway for low-frequency climate anomalies to propagate from the Labrador Sea into the mid-latitude subtropical gyre, and hence may play an important role in the thermohaline circulation and low-frequency variability of the oceanic heat content at mid-latitudes.

Acknowledgements

References

Arhan, M., 1987. On the large scale dynamics of the Mediterranean outflow. Deep-Sea Research 34, 1187–1208.

Arhan, M., de Verdière, A.C., Mèmery, L., 1994. The eastern boundary condition of the subtropical North Atlantic. Journal of Physical Oceanography 24, 1295–1316.

Armi, L., Haidvogel, D., 1982. Effects of variable and anisotropic diffusivities in a steady state diffusion model. Journal of Physical Oceanography 12, 785–794.

Armi, L., Stommel, H., 1983. Four views of a portion of the North Atlantic subtropical gyre. Journal of Physical Oceanography 13, 828–857.

Bower, A.S., Armi, L., Ambar, I., 1997. Lagrangian observations of Meddy formation during a Mediterranean Undercurrent Seeding Experiment. Journal of Physical Oceanography 27, 2545–2575.

Cunningham, S.A., Haine, T.W.N., 1995. Labrador Sea Water in the eastern North Atlantic. Part I: a synoptic circulation inferred from a minimum in potential vorticity. Journal of Physical Oceanography 25, 649–665.

Curry, R.G., 1996. HydroBase: a database of hydrographic stations and tools for climatological analysis. Woods Hole Oceanographic Instittion Technical Report WHOI-96-01, Woods Hole, MA, 50 pp.

Daniault, N., Mazé, J.P., Arhan, M., 1994. Circulation and mixing of Mediterranean water west of the Iberian Peninsula. Deep-Sea Research 41, 1685–1714.

Defant, A., 1955. Die Ausbreitung des Mittelmeerwassers im Nordatlantischen Ozean. Deep-Sea Research 465–470.

Freeland, H.J., Rhines, P., Rossby, H.T., 1975. Statistical observations of trajectories of neutrally buoyant floats in the North Atlantic. Journal of Marine Research 33, 383–404.

Gent, P.R., McWilliams, J.C., 1990. Isopycnal mixing in ocean circulation models. Journal of Physical Oceanography 20, 150–155.

Hogg, N.G., 1987. A least-squares fit of the advective-diffusive equations to Levitus Atlas data. Journal of Marine Research 45, 347–375.

Holland, W.R., Rhines, P.B., 1980. An example of eddy-induced ocean circulation. Journal of Physical Oceanography 10, 1010–1031.

Käse, R.H., Zenk, W., 1996. Structure of the Mediterranean Water and meddy characteristics in the northeastern Atlantic. In: Krauss, W. (Ed.), The Warmwatersphere of the North Atlantic Ocean, Gebrüder Borntraeger, Berlin.

Ledwell, J.R., Watson, A.J., Law, C.S., 1993. Evidence for slow mixing across the pycnocline from an open-ocean tracer-release experiment. Nature 364, 701–703.

Lozier, M.S., 1997. Evidence for large-scale eddy-driven gyres in the North Atlantic. Science 277, 361–364.

Lozier, M.S., Owens, W.B., Curry, R.G., 1995. The climatology of the North Atlantic. Progress in Oceanography 36, 1–44.

Luyten, J., Stommel, H., 1986. Gyres driven by combined wind and buoyancy flux. Journal of Physical Oceanography 16, 1151–1560.

Magnell, B., 1976. Salt fingers observed in the Mediterranean outflow region (34°N, 11°W) using a towed sensor. Journal of Physical Oceanography 6, 511–523.

Maillard, C., 1986. Atlas hydrologique de l'Atlantic Nord-Est. Institut Francais de Recherche pour l'Exploitation de la Mer., Brest, 32pp.

Mazé, J.P., Arhan, M., Mercier, H., 1997. Volume budget of the eastern boundary layer off the Iberian Peninsula. Deep-Sea Research 44, 1543–1574.

Needler, G.T., Heath, R.A., 1975. Diffusion coefficients calculated from the Mediterranean salinity anomaly in the North Atlantic. Journal of Physical Oceanography 5, 173–182.

Paillet, J., Mercier, H., 1997. An inverse model of the eastern North Atlantic general circulation and thermocline ventilation. Deep-Sea Research 44, 1293–1328.

Paillet, J., Arhan, M., McCartney, M.S., 1998. The spreading of Labrador Sea Water in the eastern North Atlantic. Journal of Physical Oceanography, in press

Pedlosky, J., 1996. Ocean Circulation Theory. Springer, Berlin, 453pp.

Richardson, P.L., Mooney, K., 1975. The Mediterranean outflow – a simple advection–diffusion model. Journal of Physical Oceanography 5, 476–482.

Richardson, P.L., McCartney, M.S., Maillard, C., 1991. A search for meddies in historical data. Dynamic and Atmospheric Oceans 15, 241–265.

Richardson, P.L., Walsh, D., Armi, L., Price, J.F., 1989. Tracking three meddies with SOFAR floats. Journal of Physical Oceanography 19, 371–383.

Saunders, P.M., 1982. Circulation in the eastern North Atlantic. Journal of Marine Research 40S, 641–657.

Schmitt, R.W., 1981. Form of the temperature-salinity relationship in the central water: Evidence for double-diffusive mixing. Journal of Physical Oceanography 11, 1015–1026.

Schopp, R., Arhan, M., 1986. A ventilated middepth circulation model for the eastern North Atlantic. Journal of Physical Oceanography 16, 344–357.

Spall, M.A., 1994. Mechanism for low-frequency variability and salt flux in the Mediterranean salt tongue. Journal of Geophysical Research 99, 10 121–10 129.

Spall, M.A., Richardson, P.L., Price, J., 1993. Advection and eddy mixing in the Mediterranean salt tongue. Journal of Marine Research 51, 797–818.

Talley, L.D., McCartney, M.S., 1982. Distribution and circulation of Labrador Sea Water. Journal of Physical Oceanography 12, 1189–1205.

Tsuchiya, M., Talley, L.D., McCartney, M.S., 1992. An eastern Atlantic section from Iceland southward across the equator. Deep-Sea Research 39, 1885–1917.

Tziperman, E., 1987. The Mediterranean outflow as an example of a deep buoyancy-driven flow. Journal of Geophysical Research 92, 14 510–14 520.

Washburn, L., Käse, R.H., 1987. Double diffusion and the distribution of the density ratio in the Mediterranean water front southeast of the Azores. Journal of Physical Oceanography 17, 12–25.

Williams, A.J., 1975. Images of ocean microstructure. Deep-Sea Research 22, 811–829.

Wüst, G., 1935. Schichtung und Zirkulation des Atlantischen Ozeans. Die Stratosphäre. Wiss. Ergebn. Dtsch. Atlant. Exped. 'meteor', 6, Teil 1, No. 2, 109–288. [English translation, The stratosphere of the Atlantic Ocean,] Emery, W.J. (Ed.), 1978, Amerind, New Delhi, 112 pp.

Young, W.R., Rhines, P.B., 1982. A theory of the wind-driven circulation II. Gyres with western boundary layers. Journal of Marine Research 40, 849–872.

Zhang, J., Schmitt, R.W., Huang, R.X., 1998. Sensitivity of GFDL Modular Ocean Model to the para-meterization of double-diffusive processes. Journal of Physical Oceanography 28, 589–605.